tvst

Article

Establishment and Characterization of a Unilateral UV-Induced Photoreceptor Degeneration Model in the C57BL/6J Mouse

Anna-Marina van der Meer[1], Tanja Berger[2], Frank Müller[3], Ann Christina Foldenauer[2,4], Sandra Johnen[1], and Peter Walter[1]

[1] Department of Ophthalmology, University Hospital RWTH Aachen, Aachen, Germany
[2] Department of Medical Statistics, RWTH Aachen University, Aachen, Germany
[3] Institute of Complex Systems, Cellular Biophysics, ICS-4, Forschungszentrum Jülich GmbH, Jülich, Germany
[4] Department of Clinical Research Fraunhofer Institute for Molecular Biology and Applied Ecology (IME) Branch for Translational Medicine and Pharmacology (TMP), Frankfurt, Germany

Correspondence: Peter Walter, Department of Ophthalmology, University Hospital RWTH Aachen, Pauwelsstr. 30, 52074 Aachen, Germany.
e-mail: pwalter@ukaachen.de

Received: May 3, 2019
Accepted: November 21, 2019
Published: August 12, 2020

Keywords: animal model; retinal degeneration; light damage; LIRD; UV-damage

Citation: Meer A-M van der, Berger T, Müller F, Foldenauer AC, Johnen S, Walter P. Establishment and characterization of a unilateral UV-induced photoreceptor degeneration model in the C57BL/6J mouse. Trans Vis Sci Tech. 2020;9(9):21, https://doi.org/10.1167/tvst.9.9.21

Purpose: To investigate whether UV irradiation of the mouse eye can induce photoreceptor degeneration, producing a phenotype reminiscent of the rd10 mouse, left eyes of female C57Bl/6J mice were irradiated with a UV LED array (370 nm). A lens was placed between the cornea and LED, allowing illumination of about one-third of the retina. The short-term and long-term effects on the retina were evaluated.

Methods: First, a dose escalation study, in which corneal dosages between 2.8 and 9.3 J/cm^2 were tested, was performed. A dosage of 7.5 J/cm^2 was chosen for the following characterization study. Before and after irradiation slit-lamp examinations, full-field electroretinography, spectral domain optical coherence tomography and macroscopy were performed. After different time spans (5 days to 12 weeks) the animals were sacrificed and the retinae used for immunohistochemistry or multielectrode array testing. Right eyes served as untreated controls.

Results: In treated eyes, spectral domain optical coherence tomography revealed a decrease in retinal thickness to 53%. Full-field electroretinography responses decreased significantly from day 5 on in treated eyes. Multielectrode array recordings revealed oscillatory potentials with a mean frequency of 5.2 $\pm$ 0.6 Hz in the illuminated area. Structural changes in the retina were observed in immunohistochemical staining.

Conclusions: UV irradiation proved to be efficient in inducing photoreceptor degeneration in the mouse retina, while leaving the other retinal layers largely intact. The irradiated area of treated eyes can be identified easily in spectral domain optical coherence tomography and in explanted retinae.

Translational Relevance: This study provides information on anatomic and functional changes in UV-treated retina, enabling the use of this model for retinitis pigmentosa-like diseases in animals suited for experimental retinal surgery.

Introduction

Retinal degenerative diseases, like retinitis pigmentosa (RP), impact the quality of life in affected patients and their relatives.[1–3] Helping these patients to preserve or regain vision is important. Electrical stimulation with retinal prostheses is one solution to tackle vision loss.[4–11] The technology has reached clinical application and patients have successfully been implanted with different devices.[12–18]

During the progression of RP, photoreceptors (PRs) degenerate while the inner retina is largely unharmed.[8] Owing to the loss of afferentiation from PRs, the layers of the inner retina undergo a process known as *remodeling*.[19] Because the retinal ganglion

cells remain intact, they are a frequent target of electrical stimulation by prostheses. By electrically stimulating ganglion cells, phosphenes can be elicited, enabling the restoration of some residual vision.[20]

To improve such retinal prostheses, large-eye animal models are needed. Aside from the well-described retinal degeneration 1 (rd1) and retinal degeneration 10 (rd10) mouse and Royal College of Surgeons rat – genetic models for RP – few genetic models exist in larger species like dog,[21] cat,[22] rabbit,[23] or miniature pig.[24] Disadvantages of genetic large species models are the slow disease progression and the lack of an intraindividual control eye. Both can be avoided by inducing PR degeneration experimentally in only one eye.

The harmful effect of light on the eye has been investigated as early as 1889[25] and the effect on the retina in more detail since the 1960s.[26] Today, it is known that light exposure can damage PRs via non thermal mechanisms. The effect on the retina depends on the duration and intensity of light exposure, wavelength, state of dark adaptation, retinal location, age, and previous light exposure, as well as the characteristics and distribution of light-absorbing chromophores.[27,28]

The fact that the retina of the rhesus monkey is most susceptible to damage by light in the UV range was found by Ham et al. in 1979.[29] This finding was confirmed in experiments with aphakic rhesus monkeys, where the retinae were six times more sensitive to light with 350 and 325 nm wavelength, than to blue light with 441 nm.[30] Van Norren et al. published similar findings obtained from rat retinae in 1990.[31] For the establishment of a PR degeneration model with an intact inner retina, it is important to know which cells are targeted by different wavelengths. In the squirrel retina, exposure to 366 nm at threshold intensity affected PRs only, whereas irradiation with 441 nm affected both, retinal pigment epithelium and PRs.[32] Gorgels et al. published related findings in pigmented Long Evans rats: in the range of 320 to 440 nm, PRs suffered the most severe damage, whereas the retinal pigment epithelium was targeted at 470 to 550 nm.[33]

According to Henriksson et al., the C57BL/6 mouse cornea transmits approximately 50 % and the lens 55 % of the radiation at 370 nm (approximated from Figures 3 and 4[34]), which are important information for calculating the retinal irradiance.

A very useful compilation of research done on light-induced retinal damage was put together by van Norren and Gorgels in 2011.[28] Extensive research on light-induced damage to the retina was also conducted by Grimm and Remé.[35–38]

Here, we report the short-term and long-term effects UV radiation had on the mouse retina and compare the produced phenotype with that of the rd10 mouse and the mouse model of n-nitroso-n-methylurea (MNU)-induced PR degeneration, before attempting to transfer the method to the large eye rabbit model. The goal is to generate a model that is characterized by PR degeneration and an intact ganglion cell layer, making it suitable for establishing surgical procedures for retinal prostheses and experiments on bridging the gap between light detection and signal transmission to the brain.

Methods

All experiments were performed in accordance with the ARVO Statement for the Use of Animals in Ophthalmic and Vision Research, the German Animal Welfare Act, and after approval was obtained by the regulatory authorities (84-02.04.2011.A386 and 84-02.04.2017.A202). All efforts were made to minimize the number of experimental animals and their suffering. Animal numbers for this study were calculated by the Department of Medical Statistics.

Experimental Design and Statistical Analysis

The experimental design was reviewed at the Department of Medical Statistics (Chair: Univ.-Prof. Dr. rer. nat. Ralf-Dieter Hilgers). For the comparison of spectral domain optical coherence tomography (sd-OCT) and full-field electroretinography (ffERG) between the treated and the untreated eye, a linear mixed effects model with point in time, eye, baseline (0d), and interaction between point in time and eye as fixed effects and animals as random effect was fitted to the data, using unstructured as covariance structure. Test results were considered statistically significant when $p < 0.05$; we adjusted for multiplicity with Holm-Scheffe procedure. Post hoc tests compared the treated and untreated eyes for fixed points in time and the points in time among each other separately for both eyes. All other outcomes were analyzed using two-sample or one-sample Student *t*-test. All statistical analyses were performed using SAS V9.4 Software (SAS Institute Inc., Cary, NC) and GraphPad Prism 6 (GraphPad Software Inc., La Jolla, CA).

In the dose escalation study, a suitable dosage of UV radiation was sought. Therefore, dosages between 2.8 J/cm^2 and 9.3 J/cm^2 were tested. Eight animals were tested with 2.8, 3.7, 5.6, 6.5, 6.5, 9.0, 9.3, and 9.3 J/cm^2. Dosages are always given as measured on the corneal surface, not on the retinal surface, if not explicitly stated otherwise.

For the calculation of retinal dosages, the following formula from[28] was used:

$$E_{ret} = E_{cor} \cdot \frac{\pi D^2}{4} \cdot \frac{\tau}{A_{ret}}$$

Corneal irradiance (E_{cor}) can be converted into retinal irradiance (E_{ret}) with D as pupil diameter (= 1.9 mm; from[39]), A_{ret} as irradiated retinal area (= 4.0 mm^2; from Fig. 2C) and τ as the transmittance of the ocular media (= 0.35; from[34]). For example, a corneal irradiance of 7.5 J/cm^2 in our case equals a retinal irradiance of 1.87 J/cm^2.

For further dosage calculation refer to Supplementary Material - Dosage Calculation.

In the dose escalation study, pre-examinations (slit lamp examination, sd-OCT, ffERG, macroscopic images) were performed. One week later, the left eye was irradiated with the respective dosage and 1, 2, and 3 weeks after the irradiation, follow-up examinations (macroscopic images, ffERG, sd-OCT) were performed. Three weeks after irradiation, the animals were sacrificed and the eyes prepared for hematoxylin and eosin (H&E) staining.

The characterization study involved four experimental groups. All groups received a pre-examination one week before irradiation (0d), involving macroscopy, ffERG, and sd-OCT. Follow-up examinations included macroscopy, ffERG, and sd-OCT as well. The groups differed in total follow-up time span (5 days, 6 weeks, 8 weeks, 12 weeks) after irradiation with 7.5 J/cm^2. Within the short-term group, animals were examined 5 days after irradiation and single animals ($n = 1$) received follow-up examinations at 1 day, 2 days, and 4 days. These single animals served to find the point in time, where one-half of the PRs were gone. For 1, 2, and 4 days after irradiation, only exemplary data are shown, because statistical evaluation was not possible. A middle term group received follow-up examinations at 1, 2, 4, and 6 weeks, and two long-term groups received follow-up examinations at 8 as well as at 8 and 12 weeks after irradiation, respectively. All animals were sacrificed in the end. The eyes of one-half of each group ($n = 4$) were prepared for multielectrode array (MEA) recordings, the other one-half ($n = 4$) for immunohistochemical stainings.

Animals

Female C57Bl/6J mice (aged 7–11 weeks, average age 8.8 ± 0.9 weeks; RRID: IMSR_JAX:000664) were housed under controlled cyclic environmental conditions (Charles River Laboratories GmbH & Co. KG, Sulzfeld, Germany: 16:8 hour light/dark cycle, < 60 lux inside the cages; animal housing facility of the Institute of Laboratory Animal Science, University Hospital RWTH Aachen, Aachen, Germany: 12:12 hour light/dark cycle, < 100 lux inside the cages) with food and water available ad libitum. All animals were obtained from Charles River Laboratories GmbH & Co. KG, Sulzfeld, Germany (https://www.criver.com/products-services/find-model/jax-c57bl6j-mice?region=23).

Anesthesia

For all experimental procedures (UV irradiation, sd-OCT, ffERG) the animals were anesthetized with an intraperitoneal injection of a mixture of xylazine (10 mg/kg xylazin 2% Bernburg, Medistar, Ascheberg, Germany) and ketamine (60 mg/kg Ketamin 10%, CEVA, Düsseldorf, Germany), 1:10 diluted in saline. For longer anesthesia periods, 0.05 mL of the ketamine-xylazine mixture were applied subcutaneously in the lumbar region every 20 minutes. The animals were kept on a heated plate at 37 °C during anesthesia to maintain body temperature. When the animals were euthanized at the end of the experiment, they were decapitated under deep ketamine/xylazine anesthesia.

Ray Tracing Simulation

The ray tracing simulation was performed at the Chair for Technology of Optical Systems (TOS; Chair: Prof. Dr. rer. nat. Loosen), using Zemax Optic Studio (15.5 SP2, ZEMAX LLC., Kirkland, WA). The light-emitting diode (LED) we used for our experiments (370 nm LED Area Light, ProPhotonix Ltd., Salem, NH) was characterized for its power at 1, 5, and 10 cm distance, using a UV sensor (UV-sensor SI1 for UV LED 395 nm, 20 mW/cm^2 + Handheld HI1 for UV sensors; UV-Technik Meyer GmbH, Ortenberg, Germany). Data on the optical properties of the mouse eye, collected from different sources were provided, to determine the beam path within the eye.[39–41] A standard plano-convex lens (LA1274-A-N-BK7 Plano-Convex Lens, $\phi = 30.0$ mm, f = 40.0 mm, AR coating: 350–700 nm; Thorlabs Inc., Newton, NJ) was inserted in the simulated beam path at different distances and the illuminated retinal area was evaluated for size and homogeneity. The LED array was equipped with a heat sink (LED area and Spot Light Heat Sink, ProPhotonix Ltd.) and a current controller (DC current controller, 0.75 A, 24 V output, StockerYale Inc., Salem, NH; operated at 0.4 A) and was additionally cooled with a standard table fan.

UV Irradiation

Before each irradiation, the UV light (AF1-370-IXF-100, Edmund Optics GmbH, Mainz, Germany; peak emission 370 ± 9 nm) was tested with a UV sensor (UV-sensor SI1 for UV LED 395 nm, 20 mW/cm^2 + Handheld HI1 for UV sensors, UV-Technik Meyer GmbH, Ortenberg, Germany) for correct intensity and possible heat generation (Checktemp I Digital Thermometer - HI98509, Hanna Instruments Deutschland GmbH, Vöhringen, Germany). For the UV irradiation of the left eye, the anesthetized mouse was repeatedly treated with mydriatic eye drops (phenylephrin 2.5 g in 10 mL, tropicamide 0.5 g in 10 mL, prepared by the pharmacy of the University Hospital Aachen, Aachen, Germany), as well as with local anesthetics (proxymetacaine hydrochloride eye drops 0.5%; Proparakain-POS, Ursapharm, Saarbrücken, Germany). The right control eye was treated with Bepanthen eye ointment (5% dexpanthenol; Bayer Leverkusen, Leverkusen, Germany) to prevent irritation and to block scattered UV light. The control eye was always turned in the opposite direction of the light source and was additionally covered by tissues. The mouse was then placed on a foam bed on a heating plate and the distance and alignment were adjusted: distance from LED housing to lens = 1 mm; distance from lens to cornea = 1 cm.

During the dose escalation study, the eyes were irradiated with 2.8 to 9.3 J/cm^2 and regularly moisturized with saline during the irradiation. After irradiation, macroscopic images of both eyes were taken. To avert pain, animals were given a subcutaneous injection of 5 mg/kg carprofen (Rimadyl, 50 mg/mL, Pfizer Deutschland GmbH, Orth a.d Donau, Germany), 1:50 diluted in physiologic saline. After irradiation and the following 3 days, the irradiated left eyes were treated with antiphlogistic eye ointment (Isopto-MAX, Alcon Pharma GmbH, Freiburg Breisgau, Germany) twice a day. During the characterization study, the eye was irradiated 8 minutes and 17 seconds, corresponding with 7.5 J/cm^2 on the corneal surface. The eye was kept moist by application of methylcellulose (Methocel 2%; Omnivision, Puchheim, Germany) every 2 minutes. Other than that, the protocol from the dose escalation study was followed. Irradiation was always performed between 2 and 4 p.m. after 1 hour of dark adaptation.

Spectral domain Optical Coherence Tomography

Sd-OCT scans were performed using the Spectralis OCT system (Heidelberg Engineering GmbH, Heidelberg, Germany) according to the protocol by Rösch et al.[42]. The infrared (InRe) image (wavelength 715 nm) of the fundus was used for localization and size estimation of the degenerated retinal area. The optic nerve head was visible in all InRe images and served as a landmark. For thickness measurements of the retina, a crosshairs was centered on the optic nerve head and thickness measurements were performed in five fixed positions (Fig. 1; Heidelberg Eye Explorer V. 1.9.13.0, 2016 Heidelberg Engineering GmbH). To evaluate whether the inner retina was affected by the UV irradiation, thickness measurements of the inner retina were analyzed. Inner retina measurements were performed from the ganglion cell layer to the outer plexiform layer in the exact same positions as measurements of the overall retinal thickness. In treated eyes, the thickness was measured exclusively in the irradiated area. Averages from the five positions were calculated and the mean values analyzed with a linear mixed effects model with point in time, eye, baseline (0d) and interaction between point in time and eye as fixed effects and animals as random effect was fitted to the data, using unstructured as covariance structure. Test results were considered statistically significant when $p < 0.05$; we adjusted for multiplicity with Holm-Scheffe procedure. Post hoc tests compared the treated and untreated eyes for fixed points in time and the points in time among each other separately for both eyes.

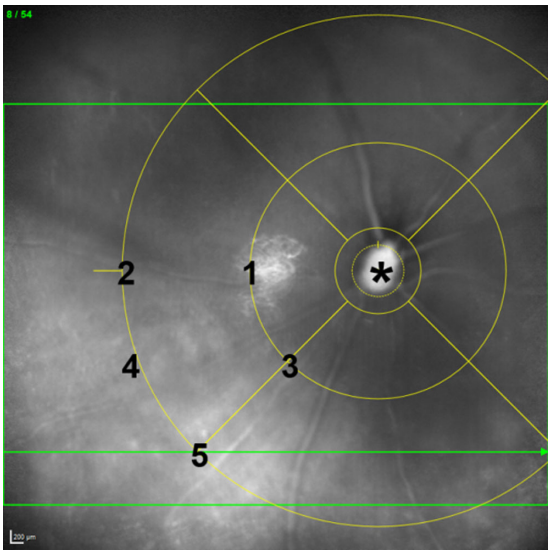

Figure 1. Positions of sd-OCT thickness measurements. InRe image of a mouse fundus. Yellow: crosshairs for fixed thickness measurement positions (1–5). *Optic nerve head.

Electroretinography

ffERG recordings were performed using the Roland Consult recording System (Roland Consult Stasche & Finger GmbH, Brandenburg a.d. Havel, Germany) as described by Rösch et al.[42] The animals were dark adapted for 1 hour before the scotopic measurements

were started. Mesopic measurements were performed right after the scotopic measurements were completed. For photopic measurements, the animal was light adapted for ≥10 minutes by illuminating the stimulator dome at 30 cd/m^2 (photopic strength). For statistical analysis, a-wave and b-wave responses were averaged from five single responses per recording. Data of scotopic (0.0095 cds/m^2, 0.476 Hz), mesopic (3.0 cds/m^2, 0.095 Hz), and photopic ffERGs (3.0 cds/m^2, 0.625 Hz) were analyzed with a linear mixed effects model with point in time, eye, baseline (0d) and interaction between point in time and eye as fixed effects and animals as random effect was fitted to the data, using unstructured as covariance structure. Test results were considered statistically significant when $p < 0.05$, and we adjusted for multiplicity with Holm-Scheffe procedure. Post hoc tests compared the treated and untreated eyes for fixed points in time and the points in time among each other separately for both eyes.

Macroscopy

Macroscopic images were taken with a Canon EOS 700D (Canon Inc., Ota, Tokio, Japan) using a macro lens (EF-S60mm f/2.8 MACRO USM) and a mounted ring flash (15 ms-1, Metz mecatech GmbH, Zirndorf, Germany) for uniform illumination.

Hematoxylin and Eosin Stainings

H&E stainings were performed according to the protocol by Rösch et al.[42,43] In brief, the eyes were enucleated, punctured twice at the *ora serrata* and fixated for 30 minutes in 4% paraformaldehyde at room temperature. The eyes were transferred to 70% ethanol and then dehydrated in a tissue dehydration automat (MTM, SLEE, Mainz, Germany) by incubation in a graded alcohol series (2 × 70%, 2 × 96%, and 3 × 100% for 1 hour), followed by xylene (3 × 1 hour) and paraffin (4 × 1 hour). After that, eyes were embedded in paraffin and 5 µm thick sections were cut with a microtome (Sliding microtome pfm Slide 4003 E, pfm medical AG, Cologne, Germany). Sections were collected in a 50 °C water bath (pfm waterbath 1000, pfm medical AG) and gathered on slides. Sections were then dried overnight at 37 °C, deparaffinated, rehydrated, and stained with hematoxylin and eosin. Sections were embedded in Vitro-Clud (R. Langenbrinck GmbH, Labor- und Medizintechnk, Emmendingen, Germany) and pictures were taken with a Leica DM IRB microscope (Leica Camera AG, Wetzlar, Germany) with a Hitachi HV-C20A camera (Hitachi Ltd.).

Immunohistochemistry

Immunohistochemistry (IHC) stainings were performed according to the protocol by Mataruga et al.[44] After fixation in 4% paraformaldehyde and cryoprotection in sucrose solution, the retina was isolated from the eye cup and the irradiated area with surrounding intact tissue cut out; 18 µm thick vertical sections were cut.

The following stainings were used: anti-protein kinase C alpha (PKC α^{rb}), anti-calcium binding protein 28K, anti-calretinin, anti-recoverin, anti-HCN1, anti-rhodopsin, anti-glial fibrillary acid protein, anti-glutamine synthetase, lectin peanut agglutinin, anti-CD11b, anti-Go-alpha, anti-HCN4, anti-PKA RIIb, anti-piccolo, and anti-mGluR6. Combinations of used primary and secondary antibodies can be found in the Supplementary Table S3, as well as dilutions and antibody sources.

In some cases, stainings were supplemented with nuclear staining by TO-PRO3 (TO-PRO3 Iodide, Thermo Fisher Scientific). TO-PRO3 (diluted 1:1000) was added to the secondary antibody incubation.

Sections were embedded in Aqua Polymount and examined with a Leica TCS confocal laser scanning microscope (Leica Microsystems, Heidelberg, Germany) with oil immersion lenses (×63/1.4). Different fluorescence channels were scanned sequentially to minimize crosstalk. Images of single confocal planes or stacks of images collapsed in the maximum projection mode were processed in ImageJ (ImageJ 1.45s, Wayne Rasband, National Institutes of Health, Bethesda, MD; RRID:SCR_003070) with the Bio-Formats add-on (ImageJ 1.45s; Bioformats 5.0.4; RRID:SCR_000450).

MEA Recordings

The tissue preparation and MEA recordings and electrical stimulation protocols from Haselier et al. were followed,[45] except that the poly-D-lysine hydrobromide treatment was not performed. Stimulus parameters used and respective responses can be found in the Supplementary Material.

The MEA with the attached retina was placed in the MEA2100-System (Multi Channel Systems MCS GmbH). The retina was immediately perfused with constantly carbogenated AMES' medium at a perfusion rate of 3 to 4 mL/min with a VC$^{(3)}$-perfusion system (ALA Scientific Instruments, Farmingdale, NY) and a peristaltic pump (Gilson Inc., Middleton, WI). Recordings were started after an acclimatization phase of 20 minutes minimum.

MEA Analysis. **Oscillations:** For the evaluation of oscillatory potentials, a 50-Hz lowpass filter was

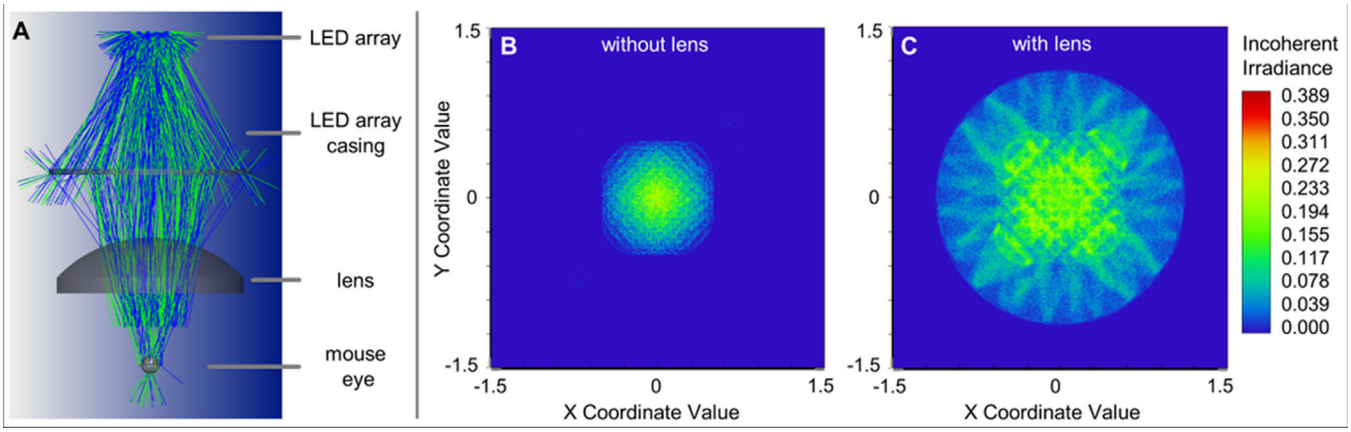

Figure 2. Ray tracing simulation with LED array and mouse eye. (A) Ray tracing alignment. Note that the illustration is not drawn to scale. Distance from LED-casing to lens: 1 mm; thickness lens: 9 mm; distance from lens to cornea: 10 mm. (B and C) Retinal surface illumination without lens (B) and with lens (C). X and Y coordinate values state the distance from the optical axis in mm. Color scale states the power on the retinal surface, starting with blue (0.000 incoherent irradiance) and increasing to red (0.389 incoherent irradiance).

applied to the raw data in MC-Rack. Files were then converted to a .txt file with the MC-DataTool (2.6.15, Multi Channel Systems MCS GmbH, Reutlingen, Germany). A fast Fourier transformation (FFT) was performed with a custom MATLAB (R2016a, The MathWorks Inc., Natick, MA) script (written by Dr. Janis Brusius, Institute of Complex Systems 8, Forschungszentrum Jülich, Germany). Dominant frequencies of one animal, measured at different electrodes, were taken into account for the calculation of a median. The medians of single animals from one group (5 days and 6, 8, and 12 weeks; one median per animal) were then treated as single measurements and used for unpaired *t*-tests to compare the four groups (5 days and 6, 8, and 12 weeks).

Results

Ray Tracing Simulation. Measurements of the UV LED array at different distances revealed intensities between 2 mW/cm^2 at 10 cm distance and 12.5 mW/cm^2 at 1 cm distance. For the simulation with the inserted lens (Fig. 2A), a distance of 1 mm from the LED casing and 10 mm from the mouse cornea resulted in a homogenous illumination of about 25% of the whole retina (Fig. 2C), being the best possible outcome with standard lenses tested. Note that absorption of ocular media (cornea, aqueous humor, lens, vitreous humor) was not accounted for in ray tracing simulations.

Dose Escalation Study. The dose escalation study taught us that, with increasing dosage, the diameter of the irradiated area of the retina increased, yet no notable additional damage was induced in other retinal layers, as shown in Figure 3A, B, as well as Figure 4. This could be observed in sd-OCT scans as well as in H&E stainings. Based on H&E stainings, sd-OCT InRe images and MEA recordings from irradiated retinae, the diameter of the irradiated retinal area was estimated to be approximately 1500 µm at dosages between 6.5 J/cm^2 and 9.3 J/cm^2. The light beam was not always exactly centered on the optic nerve head, which was especially visible at lower dosages where the diameter of the degenerated area was smaller (Fig. 3A).

Because we did not want to risk damage to the inner retinal layers and/or the retinal pigment epithelium with even higher dosages,[46,47,33] but rather aimed for a large area with degenerated PRs, we decided that the ideal dosage of UV radiation lay between 6.5 J/cm^2 and 9.3 J/cm^2, primarily based on H&E stainings, that allowed the most detailed impression. Hence, we performed irradiations in the characterization study with 7.5 J/cm^2.

We found that neovascularization of the cornea could arise if the eye was moisturized with saline during irradiation. The treatment of neovascularization with Isopto-MAX eye ointment did not always lead to an improvement, probably because the mice were trying to clean off the ointment immediately after application, thereby further irritating the eye. Neovascularization of the mouse cornea after UV irradiation has been observed before by Vangsted, who reported that long-term irradiation with a maximum dosage of 320 J/cm^2 led to a similar effect as observed in our dose escalation study.[48] Occurrence of neovascularization was not dependent on UV dosage (Figs. 3C–F), thus, we assumed that the precorneal film could not be maintained sufficiently by saline application. Dry eye is known to lead to neovascularization.[49]

In the following experiments, Methocel – that has a very similar refractive index as the cornea (Methocel:

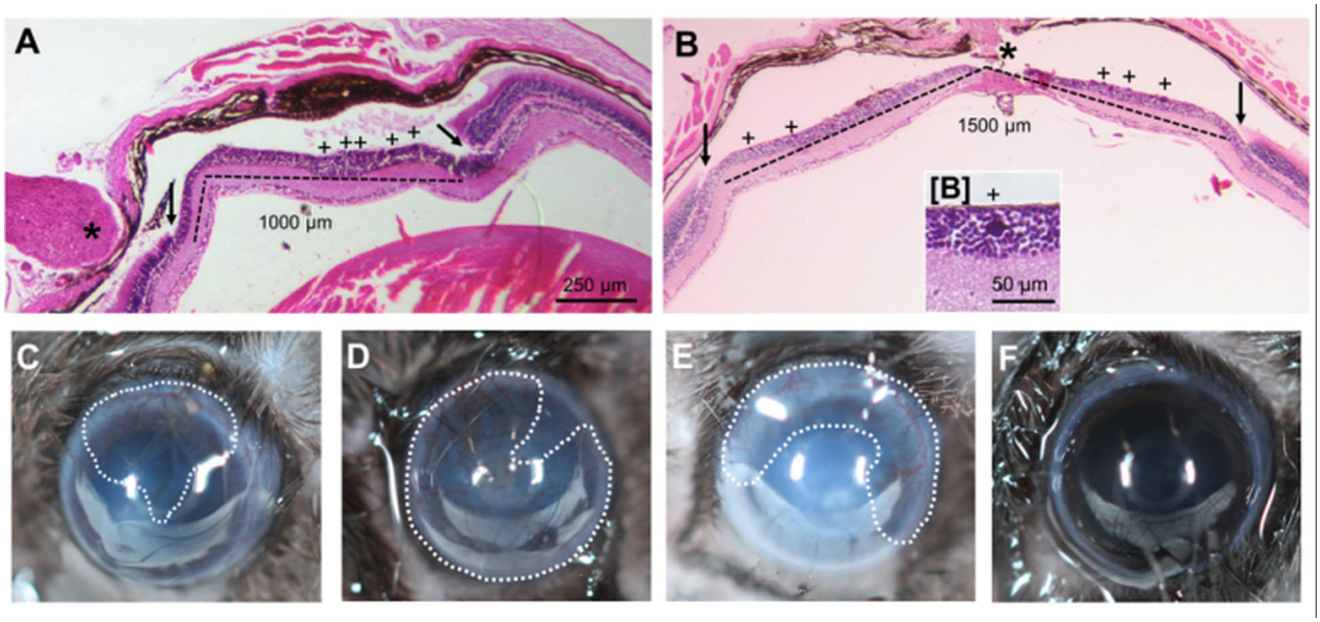

Figure 3. Dose escalation study: H&E stainings and macroscopic images. A and B: H&E stainings of eyes irradiated with 2.8 J/cm^2 (A) and 9.3 J/cm^2 (B). * = optic nerve head; arrows indicate transition from intact to irradiated area; crosses mark positions of "basophilic inclusions" (see insert [B]: higher magnification of a "basophilic inclusion" in another position); dashed line = width of irradiated area: approx. 1000 µm in A, approx. 1500 µm in B. **C,D,E,F**: macroscopic images of eyes irradiated with 5.6 (C), 9.0 (D), 9.3 (E) and 7.5 J/cm^2 (F) 4 weeks after irradiation. Dashed lines encircle neovascularized areas (C,D,E). Macroscopic images C, D and E are from the dose escalation study (eyes were moisturized with saline during irradiation), image F shows an eye from the characterization study (eyes were moisturized with Methocel during irradiation). No neovascularization was observed under these conditions.

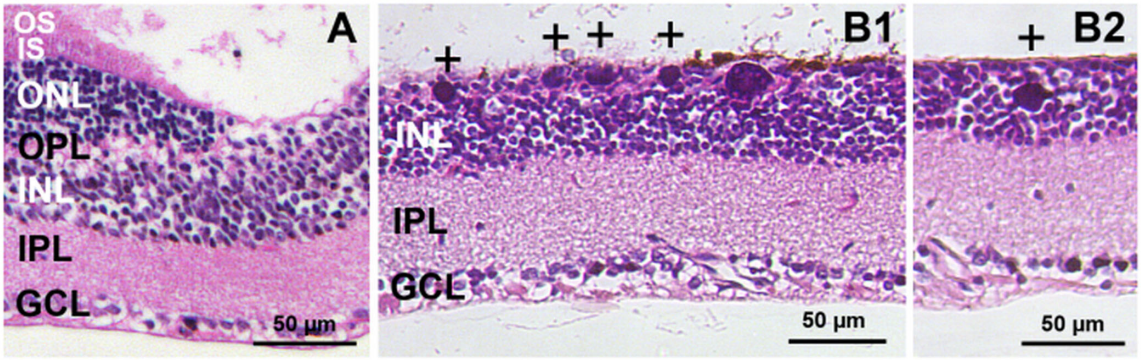

Figure 4. High magnification H&E stainings of the retinal layers of treated eyes of the dose escalation study. H&E staining of eyes irradiated with 2.8 J/cm^2 (A) and 9.3 J/cm^2 (B). The images correspond with the same animals as depicted in Figure 3A and B. GCL, ganglion cell layer; INL, inner nuclear layer; IPL, inner plexiform layer; IS, inner segments; OPL, outer plexiform layer; OS, outer segments.

1.336[50]; mouse cornea: 1.3)[40] – was chosen for moisturizing the eye during irradiation. Methocel application every 2 to 3 minutes proved to be sufficient to avoid neovascularization (Fig. 3F).

Spectral domain Optical Coherence Tomography. In sd-OCT scans, we were able to follow the progression of the degeneration process. Please note that for measurements at 1, 2, and 4 days only one animal was examined each. These points in time only served to find the point in time where about 50 % of PRs were gone. Although the data of those animals is not reliable ($n = 1$), it is described here and included in Figure 5A as exemplary data.

One day after irradiation, the effect of UV irradiation was already visible. As shown in Figure 5, in InRe as well as in cross-sectional (CS) images the transition from intact to irradiated areas could be readily

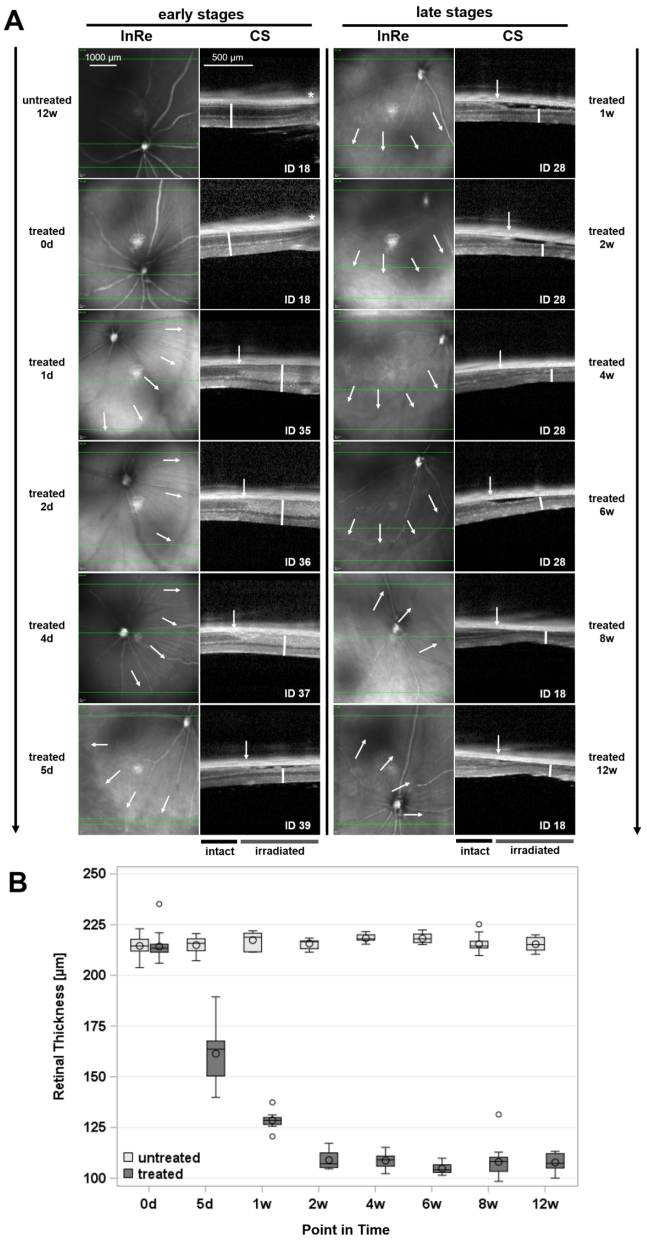

Figure 5. Time course of PR degeneration after irradiation with 7.5 J/cm². (A) sd-OCT scans at different points in time. InRe and CS images in left (early stages) and right (late stages) columns, respectively. InRe and CS images shown side by side are from the same animal at one specific point in time. In treated eyes, the intact area in CS images is displayed in the left part of the image, the irradiated area in the right part. *White arrows* indicate the transition from intact to irradiated areas, white bars indicate retinal thickness. Animal IDs allow assignment of scans to individual animals. (B) sd-OCT thickness measurements. Measurements from untreated (*light grey*) and treated (*dark grey*) eyes at different points in time were compared. Before irradiation (0d, baseline) $n = 30$ untreated eyes and $n = 31$ treated eyes were included. Five days after irradiation: $n = 7$ untreated and treated eyes; 1, 2, 4, and 6 weeks after irradiation: $n = 7$ untreated eyes, $n = 8$ treated eyes; 8 weeks after irradiation: $n = 16$ untreated and treated eyes; 12 weeks after irradiation: $n = 8$ untreated and treated eyes; Points in time covered by more than one of the four experimental groups show cumulated data of combined groups. Data were not cumulated for statistical analysis, but statistical tests were performed with separate groups. ****$p \leq 0.0001$; ns, not significant. Exact *p*-values (after Scheffe adjustment) are stated in Supplementary Table S3.2.

Table 1. Type 3 tests of fixed effects for sd-OCT measurements - multivariable analysis. The different points in time, as well as both eyes and the interaction between point in time and eye differ significantly according to type 3 tests of fixed effects. Overall thickness refers to thickness measurements of the whole retine, inner thickness refers to thickness measurements of the inner retina only. DF, degrees of freedom

	Effect	DF	*p*-Value
Overall thickness	Point in time	6	< 0.0001
	Eye	1	< 0.0001
	Baseline	1	0.0131
	Point in time * Eye	6	< 0.0001
Inner thickness	Point in time	6	0.0040
	Eye	1	< 0.0001
	Baseline	1	0.0193
	Point in time * Eye	6	0.0003

identified and stayed visible until the maximum observation period of 12 weeks. One day after irradiation the retina seemed to be thicker than in control conditions, owing to a swelling of the outer nuclear layer (ONL). After 2 and 4 days (4d) swelling was still visible, but less pronounced, until at 5 days about 50% of the PRs were gone. We could not decide from sd-OCT scans whether the increase in thickness was due to a swelling of PR somata or due to the infiltration of the ONL by microglia that was observed in IHC (Supplementary Fig. S12). One week after irradiation, only some residual cells were found in the ONL. The ONL had completely disappeared after 2 weeks. Over the course of the following weeks, no more changes were observed in sd-OCT scans (see Fig. 5).

Statistics of whole retina thickness measurements confirmed what was found in sd-OCT images. Retinal thickness of untreated eyes did not change over the course of 12 weeks. In the treated eye, retinal thickness at 5 days and 1 week was significantly greater than at all later points in time, respectively. The multivariable analysis revealed that all tested covariables point in time, eye, baseline, and interaction between point in time and eye had a statistically significant effect on the outcome sd-OCT (Table 1). The conducted post hoc tests comparing treated and untreated eyes for fixed points in time and comparing points in time separately for each eye revealed that there are significant differences for all comparisons between treated

and untreated eyes at the same point in time. In the comparison of 5 days with later points in time in the treated eye, significant differences were found for all comparisons. Comparing 1 with 2 and 4 weeks in the treated eye suggested significant differences as well. In contrast, comparisons between later points in time within treated eyes revealed no significant differences. All comparisons with exact *p*-values (after Scheffe adjustment) are stated in Supplementary Table S3.2. The mean retinal thickness of untreated eyes of all individuals over all points in time was 215 ± 3.8 µm. In treated eyes, the mean thickness declined to 161 ± 15.7 µm at 5 days, further decreased to 128 ± 4.8 µm at 1 week and stabilized at 108 ± 5.0 µm at 2 weeks (Fig. 5).

The multivariable analysis of inner retina thickness measurements revealed that all tested covariables point in time, eye, baseline, and interaction between point in time and eye had a statistically significant effect on the outcome sd-OCT (Table 1). The conducted post hoc tests comparing treated and untreated eyes for fixed points in time and comparing points in time separately for each eye revealed that there are significant differences for 6 and 8 weeks between treated and untreated eyes at the same point in time. Comparing 5 days with 6 weeks in the treated eye suggested significant differences as well. In contrast, comparisons between other points in time within treated eyes revealed no significant differences. All comparisons with exact *p*-values (after Scheffe adjustment) are stated in Supplementary Table S3.4. The mean inner retinal thickness of untreated eyes of all individuals over all points in time was 112 ± 2.6 µm. In treated eyes, the mean thickness developed over 112 ± 1.4 µm at 5 days, 113 ± 1.3 µm at 1 week, 108 ± 1.3 µm at 2 weeks, 109 ± 1.3 µm at 4 weeks, 103 ± 1.3 µm at 6 weeks, 106 ± 0.9 µm at 8 weeks to 107 ± 1.3 µm at 12 weeks (Fig. 6).

Full-field Electroretinography. For measurements at 1, 2, and 4 days, only one animal was examined each. These points in time only served to find the point in time where about 50 % of PRs were gone. Although the data of those animals is not reliable ($n = 1$), it is described here as exemplary data.

The ffERG recordings revealed deterioration of a- and b-wave responses as soon as 1d after UV irradiation (data not shown). For scotopic and photopic ffERGs, only b-wave responses were evaluated, because a-wave responses were barely detectable. For mesopic ffERGs, a- and b-wave responses were analyzed.

The rod-driven response of ON-bipolar cells, as represented by the b-waves under scotopic conditions,[51] was decreased at all points in time after irradiation. However, even 12 weeks after irradiation, a small

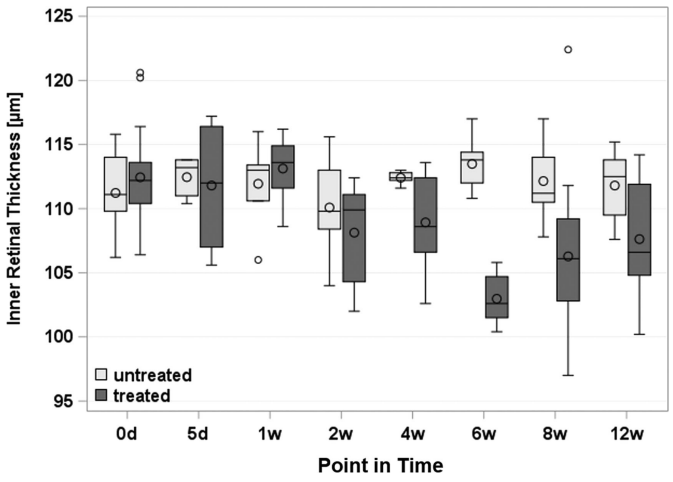

Figure 6. Thickness of the inner retina after irradiation with 7.5 J/cm². sd-OCT thickness measurements of the inner retina. Measurements from untreated (*light grey*) and treated (*dark grey*) eyes at different points in time were compared. Before irradiation (0d, baseline) $n = 30$ untreated eyes and $n = 31$ treated eyes were included. 5 days after irradiation: $n = 7$ untreated and treated eyes; 1, 2, 4, and 6 weeks after irradiation: $n = 7$ untreated eyes, $n = 8$ treated eyes; 8 weeks after irradiation: $n = 16$ untreated and treated eyes; 12 weeks after irradiation: $n = 8$ untreated and treated eyes. Points in time covered by more than one of the four experimental groups show cumulated data of combined groups. Data were not cumulated for statistical analysis, but statistical tests were performed with separate groups. Exact *p*-values (after Scheffe adjustment) are stated in Supplementary Table S3.4.

response persisted that most likely originated from the non irradiated retina (Figs. 7A, B).

The mesopic response represents a rod-dominated combined signal from PRs (a-wave) and ON-bipolar cells of both, rod and cone system (b-wave)[52] (Fig. 7A, C1, C2).

Photopic responses represent cone activity, with a-waves representing cones with post-receptoral ON-bipolar cells (b-waves).[52] A-waves were very small or undetectable in our data and therefore not further evaluated (Figs. 7A, D).

An unexpected feature was the decrease in a- and b-waves in both treated and untreated eyes 5 days after irradiation, with amplitudes considerably lower than at later points in time (Fig. 7B, C1, and C2). There also was the tendency for amplitudes of untreated eyes to slightly decrease over the course of twelve weeks. The multivariable analysis revealed that the tested covariables point in time, eye, and interaction between point in time and eye had a statistically significant effect on the outcome ffERG for scotopic and mesopic ffERGs. The tested covariable baseline was only significant for scotopic b-wave, but not for photopic b-wave or mesopic a- and b-wave (Table 2). The conducted post hoc tests comparing treated and untreated eyes for

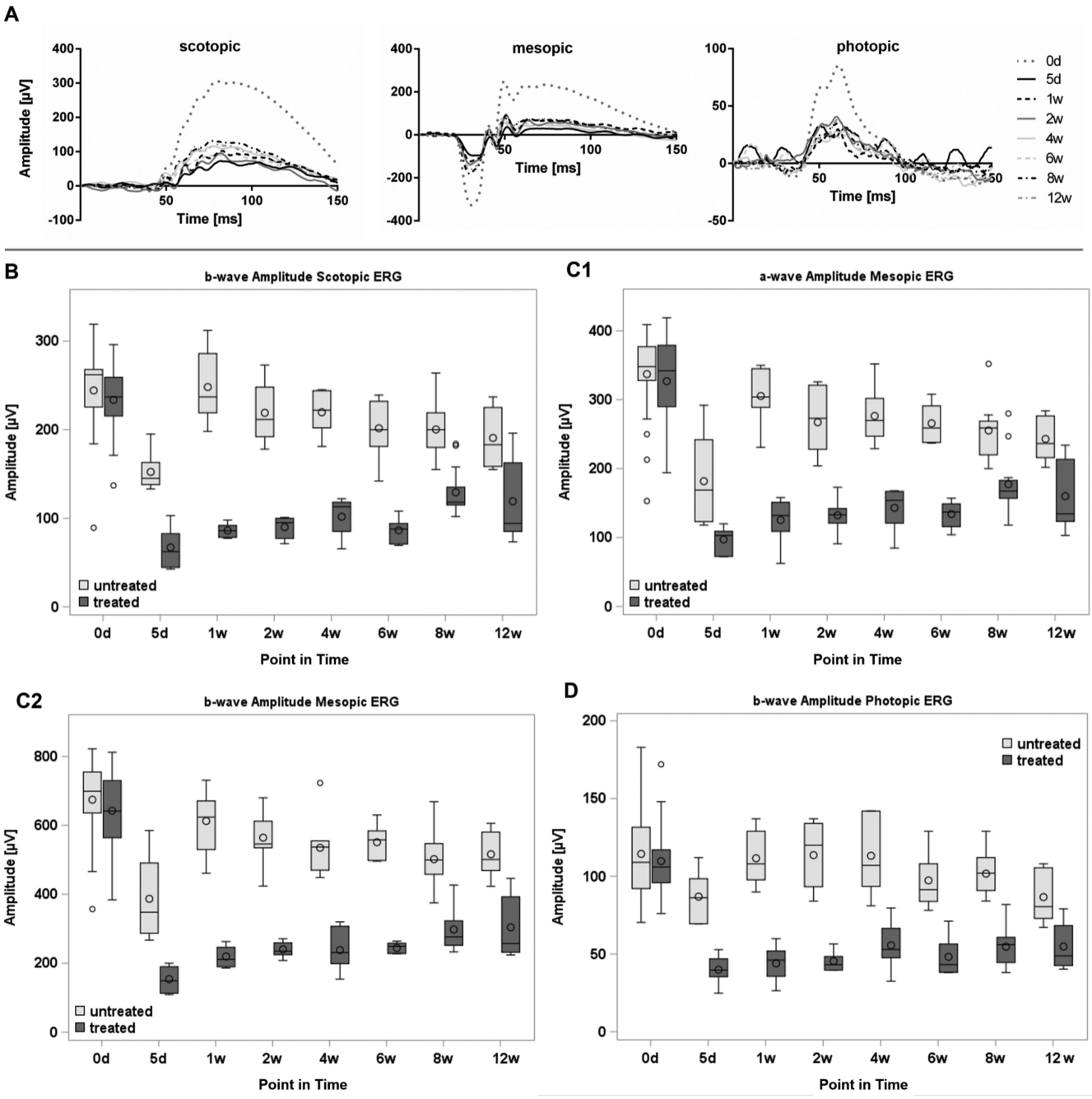

Figure 7. Development of a- and b-wave amplitudes from ffERG recordings over 12w after irradiation with 7.5 J/cm². (A) Averaged scotopic, mesopic and photopic responses are depicted. *Grey dotted traces* represent control conditions (treated eye before irradiation, 0d), the other traces represent points in time of treated eyes after irradiation: 5 days and 1, 2, 4, 6, 8, and 12 weeks. (B–D) a- and b-wave amplitudes from treated (*dark grey*) and untreated (*light grey*) eyes at different points in time. Points in time covered by more than one of the four experimental groups (0d and 8 weeks) show cumulated data of combined groups. Data were not cumulated for statistical analysis, but statistical tests were performed with separate groups. (B) Before irradiation (0d, baseline) $n = 28$ untreated and treated eyes were included, each. At 5 days and 4 and 6 weeks after irradiation: $n = 7$ untreated and treated eyes; at 1 and 2 weeks after irradiation: $n = 6$ untreated and treated eyes; at 8 weeks after irradiation: $n = 14$ untreated and treated eyes; at 12 weeks after irradiation: $n = 8$ untreated and treated eyes. (C1 and C2) At baseline: $n = 30$ untreated and treated eyes; at 5 days and 1, 2, 4, and 6 weeks after irradiation: $n = 7$ untreated and treated eyes; at 8 weeks after irradiation: $n = 14$ untreated and treated eyes; at 12 weeks after irradiation: $n = 8$ untreated and treated eyes. (D) At baseline: $n = 28$ untreated and $n = 27$ treated eyes were included. At 5 days after irradiation: $n = 6$ untreated and treated eyes; at 1 weeks after irradiation: $n = 6$ untreated and $n = 7$ treated eyes; at 2 weeks after irradiation: $n = 5$ untreated and treated eyes; at 4 and 6 weeks after irradiation: $n = 7$ untreated and treated eyes; at 8 weeks after irradiation: $n = 11$ untreated and treated eyes; at 12 weeks after irradiation: →

←

$n = 8$ untreated and treated eyes. No significant differences were found in comparisons between points in time of untreated eyes, except for the comparison 5 days vs. 1 week. Within treated eyes, no significant differences were found between the different points in time (ignoring baseline, 0d). Untreated and treated eyes did not differ at 0d (baseline), but showed significant differences at all other points in time. Different animal numbers for the recordings were the result of disturbances during single measurements. Those recordings were excluded from the data set and therefore altered the animal numbers. ****$p \leq 0.0001$; ***$p \leq 0.001$; **$p \leq 0.01$; *$p \leq 0.05$; ns $p > 0.05$. Exact p-values (after Scheffe adjustment) are stated in Supplementary Table S4.2.

Table 2. Type 3 tests of fixed effects for ERG measurements - multivariable analysis. The different points in time, as well as both eyes and the interaction between point in time and eye differ significantly according to type 3 tests of fixed effects. DF, degrees of freedom

ERG	Effect	DF	p-Value
b-wave scotopic	Point in time	6	0.0004
b-wave scotopic	Eye	1	< 0.0001
b-wave scotopic	Baseline	1	0.0099
b-wave scotopic	Point in time * Eye	6	< 0.0001
a-wave mesopic	Point in time	6	0.0016
a-wave mesopic	Eye	1	< 0.0001
a-wave mesopic	Baseline	1	0.5239
a-wave mesopic	Point in time * Eye	6	< 0.0001
b-wave mesopic	Point in time	6	0.0006
b-wave mesopic	Eye	1	< 0.0001
b-wave mesopic	Baseline	1	0.3580
b-wave mesopic	Point in time * Eye	6	0.0003
b-wave photopic	Point in time	6	0.2284
b-wave photopic	Eye	1	< 0.0001
b-wave photopic	Baseline	1	0.6126
b-wave photopic	Point in time * Eye	6	< 0.0567

fixed points in time and comparing points in time separately for each eye suggested significant differences for all comparisons between treated and untreated eyes at the same point in time (exception: 12 weeks in photopic measurements). In the comparison of 5d and 1w in the untreated eye, a significant difference was found as well (exception: photopic measurements), but all other comparisons suggested that there are no significant differences. All comparisons with exact p-values (after Scheffe adjustment) are stated in Supplementary Table S4.2.

Immunohistochemistry. In general, the time course of PR degeneration observed in IHC matched that observed in sd-OCT. Furthermore, in none of the stainings we detected clear differences between sections from 6, 8, and 12 weeks, indicating that most of the remodeling process is completed 6 weeks after irradiation at the latest and that only minor changes might occur later on.

Please note that for measurements at 1, 2, and 4 days, only one animal was examined each. Although the data of those animals is not reliable ($n = 1$), it is described here as exemplary data.

Stainings shown in Figure 8 were performed with the same antibody combinations that we have used in previous work on retinae of rd10 mouse[42] and of MNU-treated mice,[43] enabling us to compare the histology of the three models.

We observed a sharp transition between irradiated and non irradiated retina 5 days after irradiation (Fig. 8, arrow). In the irradiated area, the ONL was strongly reduced in thickness and no intact outer segments (OSs) were observed in the staining against recoverin and rhodopsin (green, blue). Only some remains of rod OSs and end feet were found (green). In TO-PRO3 stainings (labeling of nucleic acids) 5 days after irradiation the nuclei of remaining PRs looked altered (data not shown), probably owing to DNA disorganization, induced by oxidative stress (see discussion).

Glial fibrillary acidic protein (GFAP) immmunoreactivity (Fig. 8, green) revealed that Müller cells were reactive, typical for the onset of PR degeneration. In short term retinae (1–5 days after irradiation), the tissue seemed to be softer and more vulnerable, compared with later stages, making preparation and sectioning difficult (note that tissue preservation was not optimal in the 5-days sections: The tissue was fixed just as the samples of later points in time, but was more difficult to handle because it was softer and more unstable).

At 6 weeks, in the treated area, rod bipolar cells (anti-protein kinase C [PKC] α, green) had lost their dendrites but seemed otherwise intact, amacrine cells labeled against calretinin (blue) seemed normal (Fig. 8). The characteristic stratification observed in the calretinin staining (three bands in the inner plexiform layer) was preserved in irradiated retinae at all points in time (5 days and 6 weeks in Fig. 8). Horizontal cells (strongly magenta labeled cells at the outer margin of the inner nuclear layer) were missing in the irradiated area. Only punctate recoverin staining was observed while rod OSs labeled against rhodopsin and recoverin appeared healthy in the neighboring untreated area

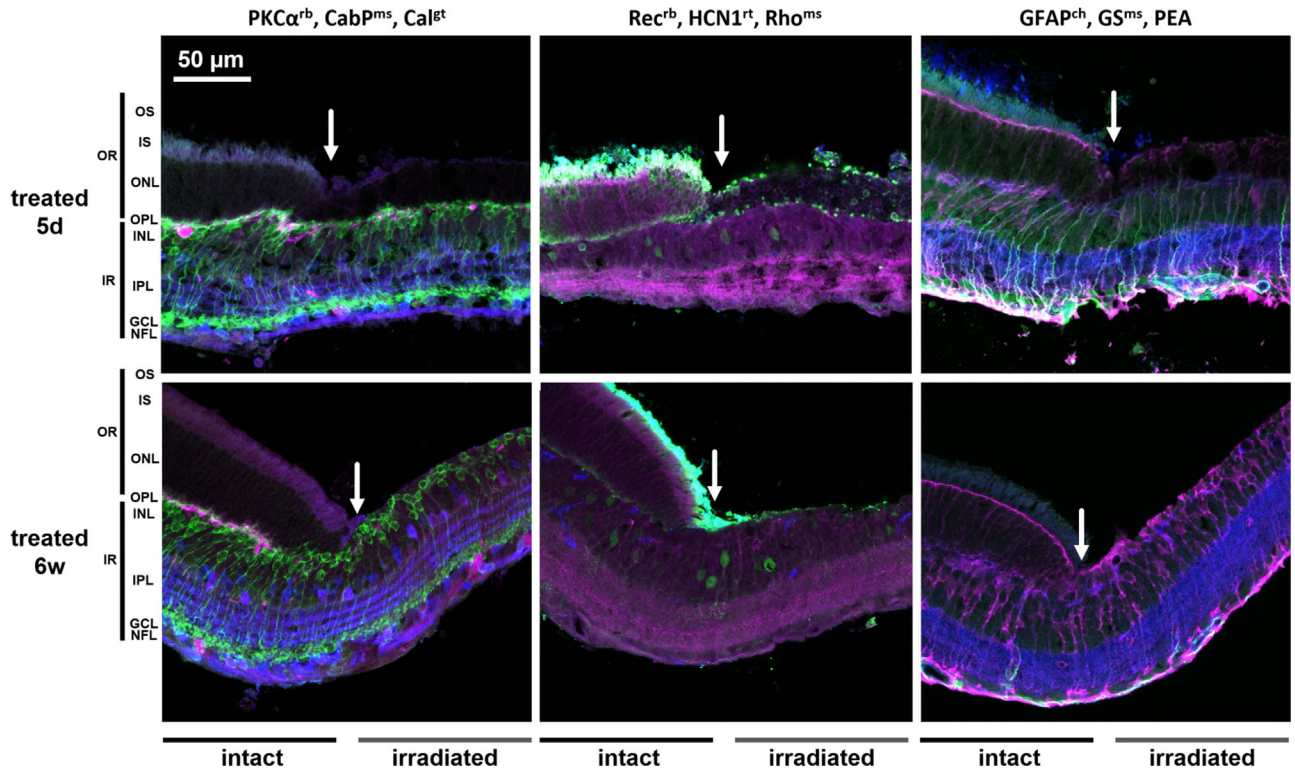

Figure 8. IHC stainings 5 days and 6 weeks after irradiation with 7.5 J/cm^2 at the transition zones between irradiated and non irradiated retina. All images depict parts of the retina where the transition from intact (*left* part of each picture) to irradiated (*right* part of each picture) areas of the retina is visible. *Arrows* indicate location of transition. *Left column*: anti-PKC α (*green*, rod bipolar cells), anti-CabP (*magenta*, horizontal cells), anti-Calretinin (*blue*, amacrine cells). *Middle column*: anti-Recoverin (*green*, PRs, type 2 bipolar cells), anti-HCN1 (*magenta*, PR somata, inner segment (IS), IPL processes), anti-Rhodopsin (*blue*, rod OS). *Right column*: anti-GFAP (*green*, astrocytes and reactive Müller cells), anti-GS (*magenta*, Müller cells), anti-lectin peanut agglutinin (*blue*, cone end feet, cone IS and OS. *Top row*: treated eye, 5 days after irradiation; *bottom row*: treated eye 6 weeks after irradiation – both from the characterization study. GCL, ganglion cell layer; INL, inner nuclear layer; IPL, inner plexiform layer; IR, inner retina; IS, inner segments; NFL, nerve fiber layer; OPL, outer plexiform layer; OR, outer retina; OS, outer segments.

(Fig. 8). Müller cell reactivity was over, indicated by their low GFAP expression.

We detected large round structures that we called "basophilic inclusions" based on their appearance in H&E stainings (Figs. 3A, B, [B], crosses). They were located in the outermost row of the INL, reminiscent of swollen somata (asterisks in Figs. 9B, C). They appeared blue in H&E stainings and were completely labeled by TO-PRO3, suggesting that they contained DNA, however, no nucleus could be identified. The structures were circular and up to five times the size of bipolar cell somata (compare bipolar cells and "basophilic inclusions" in Fig. 9C). They were not labeled with antibodies against recoverin (PRs) or CabP (horizontal cells), persisted for at least up to 12 weeks after irradiation and did not seem to change in size, shape or position.

Figure 9A shows a staining of rod bipolar cells (anti-PKC α , green) and all ON bipolar cells (anti-Go α , magenta) 6 weeks after irradiation. In the irradiated area, bipolar cell dendrites were missing. In the immediate neighborhood of the intact area, dendrites of ON bipolar cells were strongly elongated (arrows) indicating a reaction of bipolar cells close to the transition zone. We did not observe this effect in type 3a and type 3b OFF cone bipolar cells.

Figure 9D through E shows the organization of PR end feet. In untreated retina, three components can be observed at each rod end foot (anti-PSD95, blue: plasma membrane; anti-piccolo, magenta: ribbon; anti-mGluR6, green: mGluR6 on postsynaptic bipolar cell dendrites). Five days after irradiation, only a small fraction of synapses was left. Although some endfeet still seemed to be normal, others were disorganized.

MEA Recordings. In the isolated retina, the irradiated area could be readily distinguished from normal retina by sight (Figs. 10A–C). The electrophysiologic recordings of spontaneous activity revealed a strikingly clear transition from irradiated to non irradiated areas

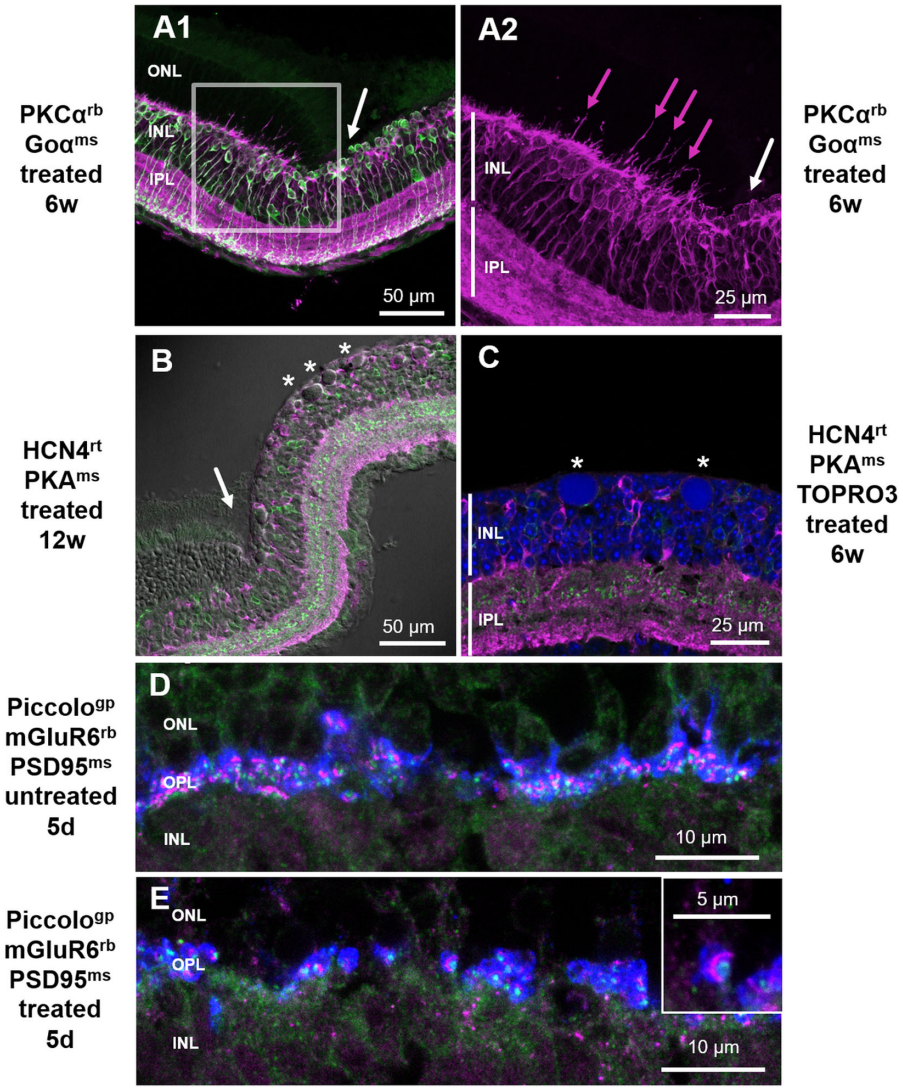

Figure 9. IHC stainings from retinae of the characterization study (7.5 J/cm^2). Anti-PKC α (*green*, rod bipolar cells), and anti-Go α (*magenta*, all ON-bipolar cells and dendritic tips). Anti-HCN4 (*green*, somata and axon terminals of type 3A cone bipolar cells), anti-PKA RIIb (*magenta*, type 3B cone bipolar cells), and TO-PRO3 (*blue*, nucleic acids, nucleus). Anti-piccolo (*magenta*, ribbon, PRs), anti-mGluR6 (*green*, dendritic tips of rod bipolar cells and all ON bipolar cells), and anti-PSD95 (*blue*, rod endfeet). (A1) Treated eye 6 weeks after irradiation. (A2) Magenta channel of A1 (*grey* frame) at higher magnification. (B) Treated eye, 12 weeks after irradiation with brightfield. (C) Treated eye 6 weeks after irradiation. (D) Untreated eye 5 days after irradiation. (E) Treated eye 5 days after irradiation. Abbreviations as in Figure 8. *White arrows* indicate location of transition from intact to irradiated retina, where both are present in one picture. *Asterisks* indicate positions of "basophilic inclusions". *Magenta arrows* highlight dendrites of bipolar cells.

(Fig. 10D). Although the intact areas showed activity typical for wildtype retina, irradiated areas displayed oscillations similar to those observed in rd1 or rd10 retina[53–56] (Figs. 10D, E). For a direct comparison, see Supplementary Figure S13.

We observed mean oscillatory frequencies of 6.0 Hz at 5 days, 4.8 Hz at 6 weeks, 5.1 Hz at 8 weeks, and 5.0 Hz at 12 weeks after irradiation. The cumulated mean of all groups was 5.2 Hz (Fig. 10F). A significant difference was only found between oscillatory frequencies at 5 days, compared with frequencies at 6 weeks. Retinae of treated eyes were also tested for light-evoked and electrically evoked responses (Supplementary Material).

Discussion

We aim for the establishment of a UV-induced PR degeneration model in the rabbit to provide for a unilateral large eye model of RP. As a first step, we established and characterized such a model in the mouse, allowing for a direct comparison with the

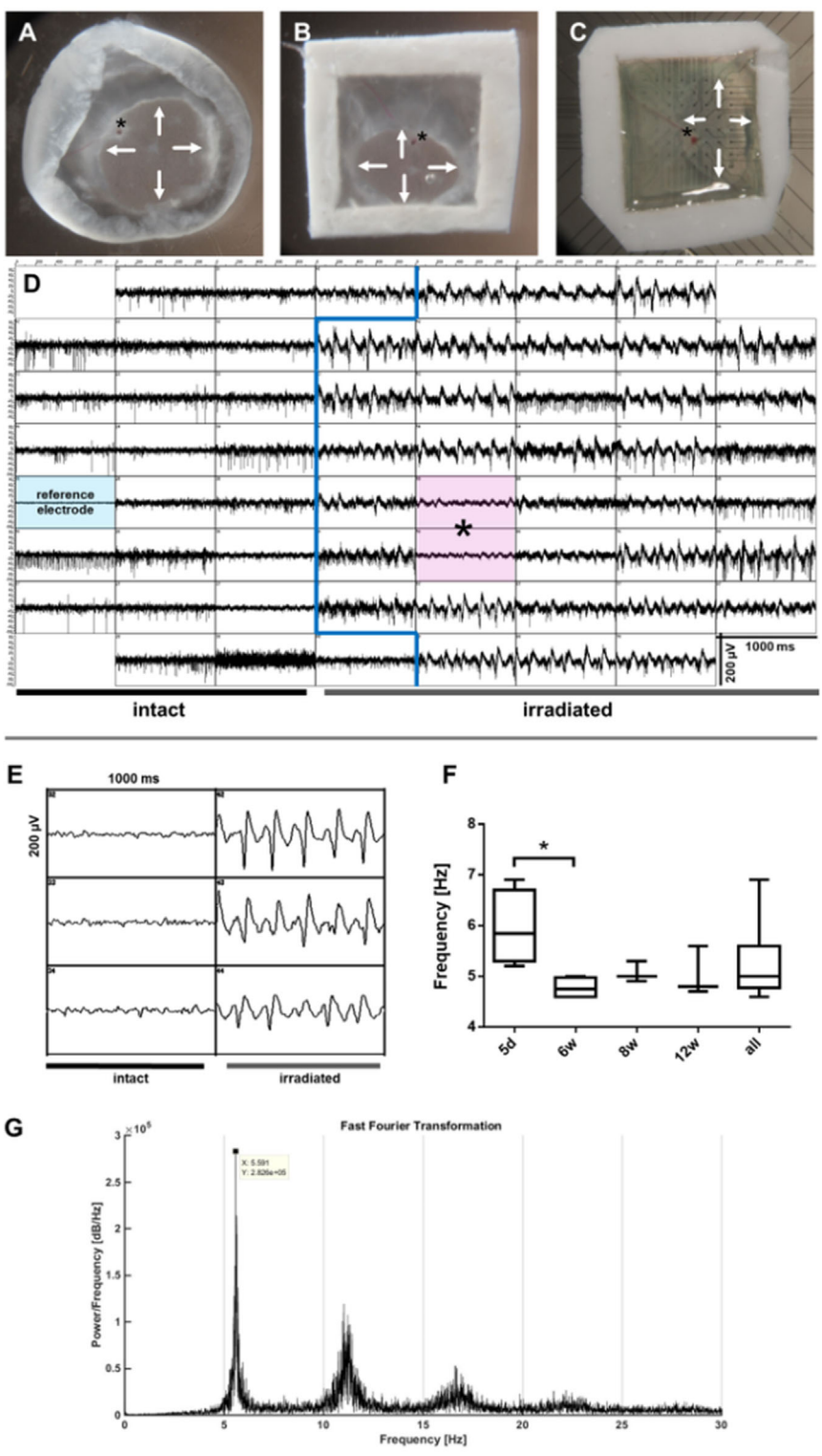

Figure 10. MEA recording of an irradiated retina 12 weeks after irradiation and FFT analysis of oscillations (7.5 J/cm^2). (A) Isolated retina with vitreous removed. (B) Isolated retina attached to nitrocellulose paper frame. (C) Isolated retina on frame attached to MEA (ganglion cells facing electrodes). *Arrows* in A, B and C indicate the border of the irradiated retinal area. (D) Raw data of MEA recording. *Blue line* indicates border between electrodes covered with intact area (*left*) and irradiated area (*right*). Asterisks indicate electrodes covering the optic nerve head. (E) A 50 Hz lowpass filtered data of the recording depicted in D, *left column* with electrodes from intact area, *right column* with electrodes from irradiated area. (F, G) FFT analysis (G) of irradiated area and box-whisker plot and statistical analysis (F) of dominant oscillatory frequencies from retinae isolated at 5 days and 6, 8, and 12 weeks after irradiation; all = cumulated data of all four groups; unpaired *t*-test was performed to compare groups; *$p \leq 0.05$. Only significant differences were visualized, all other comparisons were not significant.

genetic mouse model rd10, which is an acknowledged model for RP.

Please note that the results presented here were obtained from female mice only. It is possible that there is a gender specific effect that we missed due to our experimental setup.

In general, irradiated areas of treated eyes showed very similar characteristics as rd10 retinae in sd-OCT scans, IHC, and MEA recordings (compare).[42,55,57,58]

A striking feature of the UV-induced model was the sharp border between degenerated and intact areas of the retina in treated eyes. This was observed both on the anatomic and the electrophysiologic levels. One might have expected a smooth transition from intact to irradiated areas with decreasing layers of PRs in between, as the intensity of the UV light decreases from center to periphery (Fig. 2C). Cideciyan et al. observed a similar effect of abrupt transition in their light-exposed retinae of rhodopsin mutant dogs.[21] One explanation would be a threshold effect that allows degeneration of PRs only, if surpassed. PRs may be particularly susceptible to toxic intensities of UV light because of their high metabolic rate.[59] The high oxidative metabolism could make PRs more vulnerable to oxidative stress, because a higher amount of reactive oxygen species would be present. Reactive oxygen species are abundant in UV-exposed cells[60] and are known to have deleterious effects on a variety of cells[61–63] via diverse mechanisms.[64–66]

In ffERG recordings, we observed a reduction, but not an elimination of both a- and b-wave upon irradiation, as expected. The decline of the responses was very abrupt and fast, unlike in RP, where the responses slowly decline over time. Unexpectedly, we also found a considerable transient drop in a- and b-wave amplitude 5 days after irradiation in both treated and untreated eyes. The decrease was consistently observed in seven animals, making a random event unlikely. As of now, we do not have a sufficiently supported theory what the cause of this event might be, but a bilateral inflammatory response could explain the decrease in amplitude.[67] This finding is supported by the fact that hyperreflectivity in sd-OCT and the transient drop in ffERG responses occurred simultaneously. There also was the tendency for amplitudes of untreated eyes to slightly decrease over the course of twelve weeks. This might be an aging effect, as shown by Rösch et al.[42] Our animals from the 12 week group were 9.1 ± 1.2 weeks old at the time of irradiation, hence they were 21.1 ± 1.2 weeks old at 12 weeks after irradiation. The decline in amplitude in ffERG recordings in Rösch's work took place between postnatal weeks 12 and 24, coinciding with the slight decrease in amplitude in control eyes of our study.

Although PRs degenerated within a short time after irradiation, no major changes were observed in other cell types, except for the rapid loss of horizontal cells in the UV-induced model (Fig. 8). In the rd10 mouse, horizontal cells remain intact up to post-natal week 24,[42] but at nine months of age, approx 29% of horizontal cell somata are lost.[57] In the MNU-induced model, a difference in horizontal cell survival was found between intraperitoneal and intravitreal injection: After systemic administration of MNU and subsequent death of PRs, horizontal cells lost their dendrites, but stayed intact otherwise. After intravitreal application, horizontal cells disappeared completely at those retinal sites, at which PRs had completely degenerated.[43] Probably, horizontal cells are more susceptive to neurotoxic situations than other retinal cells. We cannot rule out that, besides the loss of synaptic input, direct effects, e.g., oxidative stress, affect the survival of horizontal cells.

We can only speculate about the nature of the "basophilic inclusions," because we did not focus on their detailed characterization. They were not living cells, because we could not find nuclei within them. It is tempting to speculate that they originated from dead horizontal cells or PRs, yet they were negative for CabP and recoverin. However, we cannot rule out that these markers were degraded during degeneration. Cideciyan et al. discovered similar structures (termed "pyknotic nuclei") in their light exposed rhodopsin mutant dog retinae.[21]

Our MEA recordings revealed a pathologic oscillatory activity in irradiated retinal areas. The frequencies observed here are in line with studies describing frequencies in other models of RP. In rd10 recordings, frequencies around 4 Hz were observed in retinae of animals aged 4 to 12 months, whereas 6 Hz were recorded in retinae of animals aged 1 to 3 months.[53] In the MNU-induced model of PR degeneration, oscillatory frequencies of 4 to 6 Hz or 3 to 9 Hz[58,45] were found. In rd1 retina, frequencies were reported to be in the range of 10 Hz.[54]

Interestingly, the sharp contour between intact and irradiated retina was not only detected on a microscopic/histologic level, but also on an electrophysiologic level, as measured with MEAs consisting of electrodes that were 200 µm apart. While we cannot rule out a smoother transition that escaped our spatial sampling, we should point out that 200 µm resolution lies in the physiologic range of ganglion cell receptive field sizes.[68,69] There is circumstantial evidence that oscillatory waves may travel in rd10 retina.[53] The sharp transition would indicate that the pathologic activity in the degenerated area cannot spread across the border into the healthy part of the retina, neither can activity

from the healthy region spread into the degenerated area and, thereby, suppress pathologic activity.

In summary, UV irradiation of the female mouse eye with 7.5 J/cm^2 leads to a reliable PR degeneration without substantially harming other ocular tissues. The UV-induced model resembles the well characterized rd10 mouse model in both morphological and electrophysiologic properties, as measured in MEA recordings. The slow decline of electrophysiologic responses over time to ffERG stimuli typical for RP could not be observed in our model, but instead the ffERG responses decreased shortly after irradiation. With a few reservations, the model presented here can serve as a model for end stage RP, with the advantage of an intraindividual control eye. However, it must be pointed out that using our experimental setup, only a part of the retina could be irradiated with UV light. By improving the custom optical apparatus, a larger retinal area might be targeted.

In a next step, this method of UV irradiation will be transferred to the rabbit, to obtain a large eye animal model. The challenge will be to find a suitable dosage for this species, as the rabbit's ocular media are qualitatively very different from those of the mouse. Cornea and lens transmit lower amounts of UV light,[70–74] and the susceptibility of the rabbit's retina could be different as well.

Acknowledgments

Ray tracing simulations were conducted in collaboration with: Prof. Dr. rer. nat. Loosen and M.Sc. Lasse Büsing; Chair for Technology of Optical Systems (TOS), Steinbachstraße 15, 52074 Aachen Christoph Aretzweiler and Stefan Esser (Institute of Complex Systems, Cellular Biophysics, ICS-4, Forschungszentrum Jülich GmbH, 52428 Jülich, Germany) were of great practical help with IHC stainings. Dr. Janis Brusius (Institute of Complex Systems, Cellular Biophysics, ICS-8, Forschungszentrum Jülich GmbH, 52428 Jülich, Germany) provided the Matlab script for FFT analyses. Dr. Kira Scherer (Institute of Laboratory Animal Science, University Hospital RWTH Aachen, Aachen, Germany) was of great assistance regarding animal testing – from gaining approval by the authorities to practical everyday considerations. This work is part of AMvdM's doctoral thesis.

Supported by Deutsche Forschungsgemeinschaft, DFG PAK 469 (SJ, FM and PW).

Disclosure: **A.-M. van der Meer,** None; **T. Berger,** None; **F. Müller,** None; **A.C. Foldenauer,** None; **S. Johnen,** None; **P. Walter,** None

References

1. Greenberg G. Beyond the blindfold: my life with retinitis pigmentosa. *Clin Dermatol*. 2005;23:640–642; discussion 642–643.
2. Rovner BW, Casten RJ. Activity loss and depression in age-related macular degeneration. *Am J Geriatr Psychiatry*. 2002;10:305–310.
3. Weyer-Wendl H, Tamm M, Walter P. Evaluation of the German version of the caregiver reaction assessment questionnaire for informal caregivers of patients with neovascular age-related macular degeneration. *Ophthalmologe*. 2015;113:230–239.
4. Majji AB, Humayun MS, Weiland JD, Suzuki S, D'Anna SA, Juan E. Long-term histological and electrophysiological results of an inactive epiretinal electrode array implantation in dogs. *Invest Ophthalmol Vis Sci*. 1999;40:2073–2081.
5. Wyatt JL, Rizzo JF, Grumet A, Edell D, Jensen RJ. Development of a silicone retinal implant: epiretinal stimulation of retinal ganglion cells in the rabbit. *Invest Ophthalmol Vis Sci*. 1994;35:1380–1380.
6. Rizzo JF, Wyatt J, Loewenstein J, Kelly S, Shire D. Methods and perceptual thresholds for short-term electrical stimulation of human retina with microelectrode arrays. *Invest Ophthalmol Vis Sci*. 2003;44:5355–5361.
7. Javaheri M, Hahn DS, Lakhanpal RR, Weiland JD, Humayun MS. Retinal prostheses for the blind. *Ann Acad Med Singapore*. 2006;35:137–144.
8. Hartong DT, Berson EL, Dryja TP. Retinitis pigmentosa. *Lancet*. 2006;368:1795–1809.
9. Scholz C. Perspectives on: materials aspects for retinal prostheses. *J Bioact Compat Polym*. 2007;22:539–568.
10. Koch C, Mokwa W, Walter P, Görtz M. First results of a study on a completely implanted retinal prosthesis in blind humans. *IEEE sensors*: 2008;1237–1240.
11. Waschkowski F, Hesse S, Rieck AC, et al. Development of very large electrode arrays for epiretinal stimulation (VLARS). *Biomed Eng Online*. 2014;13:11.
12. Roessler G, Laube T, Brockmann C, et al. Implantation and explantation of a wireless epiretinal retina implant device: observations during the EPIRET3 prospective clinical trial. *Invest Ophthalmol Vis Sci*. 2009;50:3003–3008.
13. Zrenner E, Bartz-Schmidt KU, Benav H, et al. Subretinal electronic chips allow blind patients to read letters and combine them to words. *Proc. Biol. Sci*. 2011;278:1489–1497.

14. Menzel-Severing J, Laube T, Brockmann C, et al. Implantation and explantation of an active epiretinal visual prosthesis: 2-year follow-up data from the EPIRET3 prospective clinical trial. *Eye*. 2012;26:501–509.
15. Ahuja AK, Yeoh J, Dorn JD, et al. Factors affecting perceptual threshold in Argus II retinal prosthesis subjects. *Transl Vis Sci Technol*. 2013;2:1.
16. Dorn JD, Ahuja AK, Caspi A, et al. The detection of motion by blind subjects with the epiretinal 60-electrode (Argus II) retinal prosthesis. *JAMA Ophthalmol*. 2013;131:183.
17. Stingl K, Bartz-Schmidt KU, Braun A, et al. Transfer characteristics of subretinal visual implants: corneally recorded implant responses. *Doc Ophthalmol*. 2016;133:81–90.
18. Devenyi RG, Manusow J, Patino BE, Mongy M, Markowitz M, Markowitz SN. The Toronto experience with the Argus II retinal prosthesis: new technology, new hope for patients. *Can J Ophthalmol*. 2018;53:9–13.
19. Jones BW, Marc RE. Retinal remodeling during retinal degeneration. *Exp Eye Res*. 2005;81:123–137.
20. Mohand-Said S. Selective transplantation of rods delays cone loss in a retinitis pigmentosa model. *Arch Ophthalmol*. 2000;118:807.
21. Cideciyan AV, Jacobson SG, Aleman TS, et al. In vivo dynamics of retinal injury and repair in the rhodopsin mutant dog model of human retinitis pigmentosa. *Proc Natl Acad Sci USA*. 2005;102:5233–5238.
22. May CA, Lütjen-Drecoll E, Narfström K. Morphological changes in the anterior segment of the abyssinian cat eye with hereditary rod-cone degeneration. *Curr Eye Res*. 2005;30:855–862.
23. Kondo M, Sakai T, Komeima K, et al. Generation of a transgenic rabbit model of retinal degeneration. *Investig Ophthalmol Vis Sci*. 2009;50:1371–1377.
24. Ross JW, Fernandez de Castro JP, Zhao J, et al. Generation of an inbred miniature pig model of retinitis pigmentosa. *Investig Opthalmology Vis Sci*. 2012;53:501.
25. Widmark EJ. Über den Einfluss des Lichtes auf die vorderen Medien des Auges. *Acta Physiol*. 1889;1:264–330.
26. Noell WK. Aspects of experimental and hereditary retinal degeneration. In Graymore CL, ed. *Biochemistry of the Retina*. New York: Academic Press; 1965:51–72.
27. Organisciak DT, Winkler BS. Retinal light damage: practical and theoretical considerations. *Prog Retin Eye Res*. 1994;13:1–29.
28. Van Norren D, Gorgels TGMF. The action spectrum of photochemical damage to the retina: a review of monochromatic threshold data. *Photochem Photobiol*. 2011;87:747–753.
29. Ham WT, Mueller HA, Ruffolo JJ, Clarke AM. Sensitivity of the retina to radiation damage as a function of wavelength. *Photochem Photobiol*. 1979;29:735–743.
30. Ham WT, Mueller HA, Ruffolo JJ, Guerry D, Guerry RK. Action spectrum for retinal injury from near-ultraviolet radiation in the aphakic monkey. *Am J Ophthalmol*. 1982;93:299–306.
31. Van Norren D, Schellekens P. Blue light hazard in rat. *Vision Res.* 1990;30:1517–1520.
32. Collier RJ, Zigman S. Comparison of retinal photochemical lesions after exposure to near-UV or short-wavelength visible radiation. *Prog Clin Biol Res*. 1989;314:569–575.
33. Gorgels TG, Norren D. Ultraviolet and green light cause different types of damage in rat retina. *Invest Ophthalmol Vis Sci*. 1995;36:851–863.
34. Henriksson JT, Bergmanson JPG, Walsh JE. Ultraviolet radiation transmittance of the mouse eye and its individual media components. *Exp Eye Res*. 2010;90:382–387.
35. Hafezi F, Marti A, Munz K, Remé CE. Light-induced apoptosis: differential timing in the retina and pigment epithelium. *Exp Eye Res*. 1997;64:963–970.
36. Wenzel A, Reme CE, Williams TP, Hafezi F, Grimm C. The Rpe65 Leu450Met variation increases retinal resistance against light-induced degeneration by slowing rhodopsin regeneration. *J Neurosci*. 2001;21:53–58.
37. Wenzel A, Grimm C, Samardzija M, Remé CE. Molecular mechanisms of light-induced photoreceptor apoptosis and neuroprotection for retinal degeneration. *Prog Retin Eye Res*. 2005;24:275–306.
38. Ebert S, Walczak Y, Remé C, Langmann T. Microglial activation and transcriptomic changes in the blue light-exposed mouse retina. *Adv Exp Med Biol*. 2012; 723:619–632.
39. Schmucker C, Schaeffel F. A paraxial schematic eye model for the growing C57BL/6 mouse. *Vision Res*. 2004;44:1857–1867.
40. Greiling TMS, Clark JI. The transparent lens and cornea in the mouse and zebra fish eye. *Semin Cell Dev Biol*. 2008;19:94–99.
41. Jeon CJ, Strettoi E, Masland RH. The major cell populations of the mouse retina. *J Neurosci*. 1998;18:8936–8946.
42. Rösch S, Johnen S, Müller F, Pfarrer C, Walter P. Correlations between ERG, OCT, and anatom-

ical findings in the rd10 mouse. *J Ophthalmol*. 2014;2014:874751.
43. Rösch S, Johnen S, Mataruga A, Muller F, Pfarrer C, Walter P. Selective photoreceptor degeneration by intravitreal injection of N-methyl-N-nitrosourea. *Invest Ophthalmol Vis Sci*. 2014;55:1711–1723.
44. Mataruga A, Kremmer E, Müller F. Type 3a and type 3b OFF cone bipolar cells provide for the alternative rod pathway in the mouse retina. *J Comp Neurol*. 2007;502:1123–1137.
45. Haselier C, Biswas S, Rösch S, Thumann G, Müller F, Walter P. Correlations between specific patterns of spontaneous activity and stimulation efficiency in degenerated retina. *PLoS One*. 2017;12:e0190048.
46. Collier RJ, Waldron WR, Zigman S. Temporal sequence of changes to the gray squirrel retina after near-UV exposure. *Invest Ophthalmol Vis Sci*. 1989;30:631–637.
47. Rapp LM, Smith SC. Morphologic comparisons between rhodopsin-mediated and short-wavelength classes of retinal light damage. *Invest Ophthalmol Vis Sci*. 1992;33:3367–3377.
48. Vangsted P. Alterations to eye structures in hairless mice by long-term ultraviolet irradiation - a histopathological study. *Acta Ophthalmol*. 1985;63:199–206.
49. Shinomiya K, Ueta M, Kinoshita S. A new dry eye mouse model produced by exorbital and intraorbital lacrimal gland excision. *Sci Rep*. 2018;8:1–10.
50. Swan KC. Use of methyl cellulose in ophthalmology. *Arch Ophthalmol*. 1945;33:378–380.
51. McMillan TJ, Leatherman E, Ridley A, Shorrocks J, Tobi SE, Whiteside JR. Cellular effects of long wavelength UV light (UVA) in mammalian cells. *J Pharm Pharmacol*. 2008;60:969–976.
52. McCulloch Daphne L, Marmor Michael F, Brigell Mitchell G, et al. ISCEV standard for full-field clinical electroretinography (2015 update). *Doc Ophthalmol*. 2015;130:1–12.
53. Biswas S, Haselier C, Mataruga A, Thumann G, Walter P, Müller F. Pharmacological analysis of intrinsic neuronal oscillations in rd10 retina. *PLoS One*. 2014;9:e99075.
54. Goo YS, Ahn KN, Song YJ, et al. Spontaneous oscillatory rhythm in retinal activities of two retinal degeneration (rd1 and rd10) mice. *Korean J Physiol Pharmacol*. 2011;15:415–422.
55. Jae SA, Ahn KN, Kim JY, Seo JH, Kim HK, Goo YS. Electrophysiological and histologic evaluation of the time course of retinal degeneration in the rd10 mouse model of retinitis pigmentosa. *Korean J Physiol Pharmacol*. 2013;17:229–235.
56. Toychiev AH, Ivanova E, Yee CW, Sagdullaev BT. Block of gap junctions eliminates aberrant activity and restores light responses during retinal degeneration. *J Neurosci*. 2013;33:13972–13977.
57. Gargini C, Terzibasi E, Mazzoni F, Strettoi E. Retinal organization in the retinal degeneration 10 (rd10) mutant mouse: a morphological and ERG study. *J Comp Neurol*. 2007;500:222–238.
58. Biswas S. Immunohistochemical and electrophysiological characterization of the mouse model for retinitis pigmentosa, rd10. PhD thesis, RWTH Aachen University;2014.
59. Ames A, Li Y-Y, Heher EC, Kimble CR. Energy metabolism of rabbit retina as related to function: high cost of Na+ transport. *J Neurosci*. 1992;12:840–853.
60. Tobi SE, Paul N, McMillan TJ. Glutathione modulates the level of free radicals produced in UVA-irradiated cells. *J Photochem Photobiol B Biol*. 2000;57:102–112.
61. Čejková J, Štípek S, Crkovská J, et al. UV rays, the prooxidant/antioxidant imbalance in the cornea and oxidative eye damage. *Physiol Res*. 2004;53:1–10.
62. Cejka C, Cejkova J. Oxidative stress to the cornea, changes in corneal optical properties, and advances in treatment of corneal oxidative injuries. *Oxid Med Cell Longev*. 2015;591530.
63. Giblin FJ, Leverenz VR, Padgaonkar VA, et al. UVA light in vivo reaches the nucleus of the guinea pig lens and produces deleterious, oxidative effects. *Exp Eye Res*. 2002;75:445–458.
64. Kielbassa C, Roza L, Epe B. Wavelength dependence of oxidative DNA damage induced by UV and visible light. *Carcinogenesis*. 1997;18:811–816.
65. Kvam E, Tyrrell RM. Induction of oxidative DNA base damage in human skin cells by UV and near visible radiation. *Carcinogenesis*. 1997;18:2379–2384.
66. Peak MJ, Peak JG, Jones CA. Different (direct and indirect) mechanisms for the induction of DNA-protein crosslinks in human cells by far- and near-ultraviolet radiations (290 and 405 nm). *Photochem Photobiol*. 1985;42:141–146.
67. Yoshimura N, Hangai M. *OCT Atlas*. Heidelberg, Germany: Springer Medizin; 2014.
68. DeVries SH, Baylor DA. Mosaic arrangement of ganglion cell receptive fields in rabbit retina. *J Neurophysiol*. 1997;78:2048–2060.
69. Baden T, Berens P, Franke K, Román RM, Bethge M, Euler T. The functional diversity of retinal ganglion cells in the mouse. *Nature*. 2016;529:345–350.
70. Algvere PV, Torstensson PAL, Tengroth BM. Light transmittance of ocular media in living rab-

bit eyes. *Investig Ophthalmol Vis Sci*. 1993;34:349–354.
71. Walsh JE, Bergmanson JP, Koehler LV, Doughty MJ, Fleming DP, Harmey JH. Fibre optic spectrophotometry for the in vitro evaluation of ultraviolet radiation (UVR) spectral transmittance of rabbit corneas. *Physiol Meas*. 2008;29:375–388.
72. Čejka Č, Pláteník J, Širc J, et al. Changes of corneal optical properties after UVB irradiation investigated spectrophotometrically. *Physiol Res*. 2010;59:591–597.
73. Douglas RH, Jeffery G. The spectral transmission of ocular media suggests ultraviolet sensitivity is widespread among mammals. *Proc Biol Sci*. 2014;281:20132995.
74. Tsukahara N, Tani Y, Kikuchi H, Sugita S. Light transmission of the ocular media in birds and mammals. *J Vet Med Sci*. 2014;76:93–95.